Thermal performance of flat-shaped heat pipes using nanofluids

Maryam Shafahi [a], Vincenzo Bianco [b], Kambiz Vafai [a,*], Oronzio Manca [b]

[a] Department of Mechanical Engineering, University of California Riverside, Riverside, CA 92521, USA
[b] Dipartimento di Ingegneria Aerospaziale e Meccanica, Seconda Università, degli Studi di Napoli, Via Roma 29, 81031 Aversa (CE), Italy

ARTICLE INFO

ABSTRACT

Analytical models are utilized to investigate the thermal performance of rectangular and disk-shaped heat pipes using nanofluids. The liquid pressure, liquid velocity profile, temperature distribution of the heat pipe wall, temperature gradient along the heat pipe, thermal resistance and maximum heat load are obtained for the flat-shaped heat pipes utilizing a nanofluid as the working fluid. The flat-shaped heat pipe's thermal performance using a nanofluid is substantially enhanced compared with one using a regular fluid. The nanoparticles presence within the working fluid results in a decrease in the thermal resistance and an increase in the maximum heat load capacity of the flat-shaped heat pipe. The existence of an optimum nanoparticle concentration level and wick thickness in maximizing the heat removal capability of the flat-shaped heat pipe was established.

1. Introduction

Heat pipes have been utilized in heat transfer related applications for many years. Depending on their application area, they can operate over a wide range of temperatures with a high heat removal capability. Heat pipes have been found to be useful in a number of technologies such as electronic cooling, spacecraft thermal control, transportation systems, automotive industry, permafrost stabilization, bio-related applications, solar systems and manufacturing [1–6].

Mathematical and experimental models of the transport mechanisms for flat-shaped heat pipes have been developed by Vafai and co workers [2–6] and a comprehensive analytical solution for a cylindrical heat pipe incorporating the effect of liquid–vapor coupling and non-Darcian transport was presented by Zhu and Vafai [7].

The idea of utilizing nanoparticles within the working fluid of a heat pipe has become a subject of interest in recent years [8–12]. There are a number of studies on thermal conductivity of the nanofluids [13–15]. The nanoparticles within the fluid change its thermal conductivity, viscosity and density. It has been shown experimentally that, for a given concentration level, the thermal conductivity of the nanofluids increases with a decrease in particle diameter [15–17]. However, there are some investigations which do not confirm this enhancement in the thermal conductivity [18,19].

Most of the investigations on the effect of using nanofluids within a heat pipe have been carried out experimentally. The thermal performance of a nanofluid based cylindrical heat pipe was studied analytically by Shafahi et al. [8]. In the current work, analytical models established by Vafai and co workers [3,4] are utilized to study the effect of using a nanofluid within the flat-shaped heat pipes. Disk and rectangular shaped heat pipes have substantial advantages over conventional cylindrical heat pipes. A more flexible geometry, substantially higher heat removal capability, ability to incorporate asymmetrical heating and a built in secondary transport to assimilate overload and prevent or delay a dry out are some of the advantages of the flat-shaped heat pipes analyzed by Vafai and co workers [2–6]. A wide range of nano particles such as silver [20–23], CuO [10,24], diamond [11,25], titanium [9,12], nickel oxide [26] and gold [27] have been used to study the influence of nanofluid on the heat pipe performance. It has been observed experimentally that the heat pipe thermal resistance [11,12,20,22–24,27] and temperature gradient [20,23,25] decrease when using a nanofluid as the working fluid.

In this work, a comprehensive analytical solution for disk and rectangular shaped heat pipes [2,4] has been modified to incorporate the presence of nanoparticles within the working fluid. The liquid pressure and velocity profile, temperature distribution, temperature gradient along the heat pipe, thermal resistance and maximum heat removal capability are obtained for different concentration levels of nanoparticles within flat-shaped heat pipes. Three of the most common types of nanoparticles namely Al_2O_3, CuO, and TiO_2 are considered in this work. There is substantial enhancement in thermal performance of a flat-shaped heat

* Corresponding author.
E-mail address: vafai@engr.ucr.edu (K. Vafai).

Nomenclature

A_c	condenser area [m^2]
A_e	evaporator area [m^2]
A_{tot}	total external surface area of the heat pipe [m^2]
$f(x)$	position of maximum value of vapor velocity in y direction [m]
h	convective heat transfer coefficient [W/m^2 K]
h_b^+	dimensionless half width of any of the vapor channels
h_v	height of vapor space for the heat pipe [m]
h_{tot}	thickness of the heat pipe [m]
h_w	thickness of the wick [m]
h_w^+	dimensionless thickness of the wick $\left(\frac{h_w}{h_v}\right)$
K	permeability of the wick [m^2]
K^+	dimensionless permeability $\left(K^+ = \frac{K}{h_w^2}\right)$
k	thermal conductivity [W/m K]
k_{eff}	effective thermal conductivity of the liquid saturated wick [W/m K]
k_{layer}	nanolayer thermal conductivity [W/m K]
k_{wall}	thermal conductivity of the heat pipe wall [W/m K]
l	length of the rectangular shaped heat pipe [m]
l^+	dimensionless length of the rectangular shaped heat pipe
p	pressure [Pa]
p_l	liquid pressure [Pa]
p_l^+	dimensionless liquid pressure
p_v	vapor pressure [Pa]
p_v^+	dimensionless vapor pressure
Q_{max}	maximum heat input [W]
r	dimensional radial coordinate [m]
r^+	dimensionless radial coordinate
r_p	nanoparticles radius [nm]
r_c	effective pore radius of the wick [m]
R	radius of the disk-shaped heat pipe [m]
R^+	dimensionless radius of the disk-shaped heat pipe
R_t	heat pipe's thermal resistance [K/W]
Re_h	injection Reynolds number $(v_1 h_v / v_v)$
T	temperature [K]

T_b	bulk temperature [K]
u_l	liquid velocity [m/s]
v_1	vapor injection velocity [m/s]
v_1^+	dimensionless vapor injection velocity $(v_1 h_v / v_v)$
v_2	vapor suction velocity [m/s]
v_2^+	dimensionless vapor suction velocity $(v_2 h_v / v_v)$
w	nanolayer thickness [nm]
x	dimensional coordinate for the rectangular shaped heat pipe [m]
x^+	dimensionless coordinate for the rectangular shaped heat pipe

Greek symbols

ϕ	particle concentration
ε	porosity of the wick
μ	dynamic viscosity [N s/m^2]
v	kinematic viscosity [m^2/s]
μ^+	dimensionless dynamic viscosity
ρ	density [kg/m^3]
ρ^+	dimensionless density $(\frac{\rho_l}{\rho_v})$
σ_l	surface tension of the working fluid [N/m]

Subscripts

0	heat pipe with pure fluid
bf	base fluid
l	liquid phase
max	maximum
nf	nanofluid
p	particle
v	vapor
w	wick

Superscript

+	dimensionless quantity

pipe utilizing a nanofluid. The effect of nanoparticle size on the performance of the flat-shaped heat pipe is investigated and it is shown that smaller nanoparticles produce the most enhancement in the thermal performance of a heat pipe. The maximum heat capability is established for various wick thicknesses and nanoparticle concentrations and the potential for reducing the size of a heat pipe for a given heat load by utilizing a nanofluid is studied. Our results demonstrate the existence of an optimum concentration level and wick thickness for maximizing the heat removal capability of a flat-shaped heat pipe.

2. Analysis and formulation

A simplified schematic of a rectangular or disk-shaped heat pipe's cross section is shown in Fig. 1. It is assumed that vapor and liquid flow are steady and laminar and transport properties of the vapor and liquid are considered to be constant; the vapor injection and suction rates are considered to be uniform in the evaporator [2].

2.1. Pressure distribution

Pressure distribution is obtained by integrating the momentum equation while applying the appropriate boundary conditions [2,4]. This results in the following expressions for the vapor and liquid pressure distribution in disk and rectangular shaped heat pipes respectively.

2.1.1. Disk-shaped heat pipe's vapor pressure distribution

$$p_v^+(r^+) = \begin{cases} p_v^+(0) - \frac{24}{25}\left(\frac{1-\lambda^2}{2-\lambda^2}Re_h R^+\right)^2\left(\frac{r^+}{R^+}\right)^2 & 0 \le r^+ \le \lambda R^+ \\ p_v^+(0) - \frac{8}{25}\left(\frac{\lambda^2}{2-\lambda^2}Re_h R^+\right)^2\left[3\left(\frac{r^+}{R^+}\right)^2 + \left(\frac{R^+}{r^+}\right)^2 - 4\ln\frac{r^+}{R^+}\right. \\ \left. -2\left(3-2\ln\lambda-\frac{1}{\lambda^2}\right)\right] & \lambda R^+ \le r^+ \le R^+ \end{cases}$$

(1)
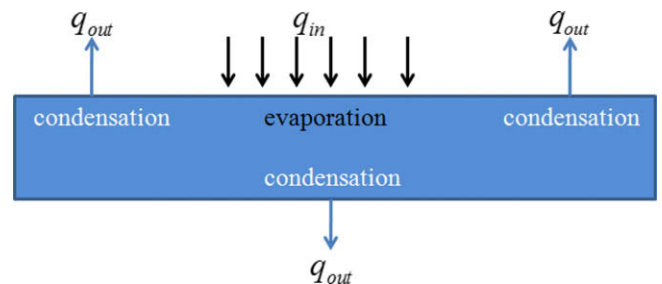
Fig. 1. Simple schematic of rectangular or disk- shaped heat pipe's cross section.

where λ is the square root of the ratio of the evaporator area to the total area: $r^+ = \frac{rv_v}{h_v^2 v_1}$ and $p_v^+ = \frac{p_v}{\rho_v v_1^2}$ for the disk-shaped heat pipe.

2.1.2. Rectangular shaped heat pipe's vapor pressure distribution

The vapor flow in the rectangular shaped heat pipe does not have a symmetrical velocity profile. The maximum vapor velocity position moves towards the lower plate due to vapor injection from the upper wall. An approximate solution for f^+ is obtained using Bernoulli's equation [2]:

$$\frac{df^+(x^+)}{dx^+} = \begin{cases} \left[-\frac{9}{2}(1-\lambda)f^+(x^+) + 5\frac{(2-\lambda)}{Re_h}\frac{1}{f^+(x^+)} - \frac{5}{2}\lambda \right]\frac{1}{(1-\lambda)x^+} \\ \quad 0 < x^+ \leq \lambda l^+ \\ \left[-\lambda f^+(x^+) + 10\frac{(2-\lambda)}{Re_h}\frac{1}{f^+(x^+)} \right]\frac{1}{7\lambda(l^+ - x^+)} \\ \quad l^+ \leq x^+ < l^+ \end{cases} \tag{2}$$

where the dimensionless coordinate for rectangular shaped heat pipe's vapor phase is $x^+ = \frac{v_v x}{h_v^2 U_{ov}}$ and U_{ov} is the maximum vapor velocity.

As such the vapor pressure distribution can be presented as:

$$\Delta p_v^+(x^+) = \begin{cases} -\frac{4(1-\lambda)}{(2-\lambda)}Re_h \left(\begin{array}{c} \left[\frac{16(1-\lambda)}{25(2-\lambda)}Re_h + \frac{1}{2(h_v^+)^2} \right](x^+)^2 \\ + \int_0^{x^+} \frac{x^+}{f^+(x^+)(1 - f^+(x^+))} dx^+ \end{array} \right) \\ \quad 0 \leq x^+ \leq \lambda l^+ \\ \Delta p_v^+(\lambda l^+) - \frac{4\lambda}{(2-\lambda)}Re_h \left(\begin{array}{c} \left[\frac{16\lambda}{25(2-\lambda)}Re_h - \frac{1}{2(h_v^+)^2} \right]\left[(x^+ - l^+)^2 - (\lambda l^+ - l^+)^2 \right] \\ - \int_0^{x^+} \frac{x^+ - l^+}{f^+(x^+)(1 - f^+(x^+))} dx^+ \end{array} \right) \\ \quad \lambda l^+ \leq x^+ < l^+ \end{cases} \tag{3}$$

where dimensionless vapor pressure is $p_v^+ = \frac{p_v}{\rho_v U_{ov}^2}$ and λ is the ratio of the evaporator length to the heat pipe length for the rectangular shaped heat pipe.

The liquid pressure distribution for the rectangular and disk-shaped heat pipes can be presented as [2,4]:

2.1.3. Disk-shaped heat pipe's liquid pressure distribution

$$p_l^+(r^+) = \begin{cases} p_v^+(0) + \frac{v^+ Re_h (R^+)^2}{4K^+ (h_w^+)^3}\frac{1-\lambda^2}{2-\lambda^2}\left[\left(\frac{r^+}{R^+}\right)^2 + \frac{2\lambda^2}{1-\lambda^2}\ln\lambda \right] \\ \quad -\left(\frac{4}{5}\frac{\lambda^2}{2-\lambda^2}Re_h R^+ \right)^2 \left(2\ln\lambda + \frac{1}{\lambda^2} - 1 \right) \quad 0 \leq r^+ \leq \lambda R^+ \\ p_v^+(0) + \frac{v^+ Re_h (R^+)^2}{4K^+ (h_w^+)^3}\frac{\lambda^2}{2-\lambda^2}\left(1 - \left(\frac{r^+}{R^+}\right)^2 - 2\ln\left(\frac{R^+}{r^+}\right) \right) \\ \quad -\left(\frac{4}{5}\frac{\lambda^2}{2-\lambda^2}Re_h R^+ \right)^2 \left(2\ln\lambda + \frac{1}{\lambda^2} - 1 \right) \quad \lambda R^+ \leq r^+ \leq R^+ \end{cases} \tag{4}$$

where dimensionless liquid pressure is $p_l^+ = \frac{p_l}{\rho_l v_1^2}$ and $v^+ = \frac{v_l}{v_v}$ for disk-shaped heat pipe.

2.1.4. Flat-shaped heat pipe's liquid pressure distribution

$$\Delta p_l^+(x^+) = \begin{cases} \Delta p_v^+(l^+) - \frac{h_w^+ \mu^+(1-\lambda)Re_h}{2(2-\lambda)K^+}\Big\{ \lambda(1-\lambda)(l^+)^2 \\ \quad + \left[(\lambda l^+)^2 - (x^+)^2 \right] \Big\} \quad 0 \leq x^+ \leq \lambda l^+ \\ \Delta p_v^+(l^+) - \frac{h_w^+ \mu^+ \lambda Re_h}{2(2-\lambda)K^+}(l^+ - x^+)^2 \quad \lambda l^+ \leq x^+ \leq l^+ \end{cases} \tag{5}$$

where $\mu^+ = \frac{\mu_v}{\mu_l}$; the dimensionless coordinate for the rectangular shaped heat pipe's liquid phase is $x^+ = \frac{v_l x}{U_{ol} h_w^2}$ and U_{ol} is maximum liquid phase velocity. It can be seen that liquid pressure is related to the liquid viscosity which is affected when using nanoparticles within the working fluid. The classical Brinkman model [28] is used to obtain the nanofluid viscosity:

$$\mu_{nf} = \frac{\mu_{bf}}{(1-\phi)^{2.5}} \tag{6}$$

where μ_{bf} is the viscosity of the base fluid which is water for our investigation. Nanofluid's density is calculated based on a simple representation of the particle and fluid phases proposed by Pak and Cho [29].

$$\rho_{nf} = \rho_p \phi + (1-\phi)\rho_{bf} \tag{7}$$

where ρ_{nf}, ρ_p and ρ_{bf} are the nanofluid, particle and base fluid densities respectively.

2.2. Velocity distribution

Using Darcy's and applying the mass balance for the lower and upper wicks the liquid velocity distribution for the rectangular and disk-shaped heat pipes can be presented by [2,4]:

Liquid velocity distribution for the disk-shaped heat pipe:

$$u_l^+(r^+) = \begin{cases} \frac{v_1^+ - v_2^+}{4\rho^+ h_w^+}r^+ & 0 \leq r^+ \leq \lambda R^+ \\ -\frac{v_2^+}{2\rho^+ h_w^+}\frac{(r^+)^2 - (R^+)^2}{r^+} & \lambda R^+ \leq r^+ \leq R^+ \end{cases} \tag{8}$$

where $\rho^+ = \rho_l / \rho_v$.

Liquid velocity distribution for the rectangular shaped heat pipe:

$$u_l^+(x^+) = \begin{cases} \frac{h_w^+ \mu^+ (v_1^+ - v_2^+)}{2}x^+ & 0 \leq^+ \leq \lambda l^+ \\ h_w^+ \mu^+ v_2^+ (l^+ - x^+) & \lambda l^+ \leq x^+ \leq l^+ \end{cases} \tag{9}$$

2.3. Temperature distribution

The wall temperature profile is obtained based on the assumption of uniform temperature along the condenser and evaporator sections. Based on simple energy balances, the condenser and evaporator wall temperatures as well as the vapor temperature can be respectively presented as:

Condenser wall temperature:

$$T_{wall,c} = T_b + \frac{Q}{A_c h} \tag{10}$$

Evaporator wall temperature:

$$T_{wall,e} = T_v + \frac{Q}{A_e}\left(\frac{h_{wall}}{k_{wall}} + \frac{h_w}{k_{eff}} \right) \tag{11}$$

where h_{wall} and h_w are the wall and wick thicknesses respectively.

Vapor temperature:

$$T_v = T_b + \frac{Q}{A_c}\left(\frac{1}{h} + \frac{h_{wall}}{k_{wall}} + \frac{h_w}{k_{eff}} \right) \tag{12}$$

The heat pipe's temperature distribution is dependent on the wick thermal conductivity which can be presented as [30]:

$$k_{eff} = \frac{k_l[(k_l + k_s) - (1 - \varepsilon)(k_l - k_s)]}{[(k_l + k_s) + (1 - \varepsilon)(k_l - k_s)]} \tag{13}$$

where k_s and k_l are solid and liquid conductivities. For this work k_l is replaced with k_{nf}. It should be noted that k_{eff} increases with an increase in thermal conductivity of nanofluid. The nanofluid conductivity is obtained from Yu and Choi [31] model that can be presented as:

$$k_{nf} = \frac{k_{pe} + 2k_l + 2(k_{pe} - k_l)(1 + \beta)^3 \phi}{k_{pe} + 2k_l - (k_{pe} - k_l)(1 + \beta)^3 \phi} k_l \tag{14}$$

To account for the effect of nanolayer, solid particle conductivity is modified as
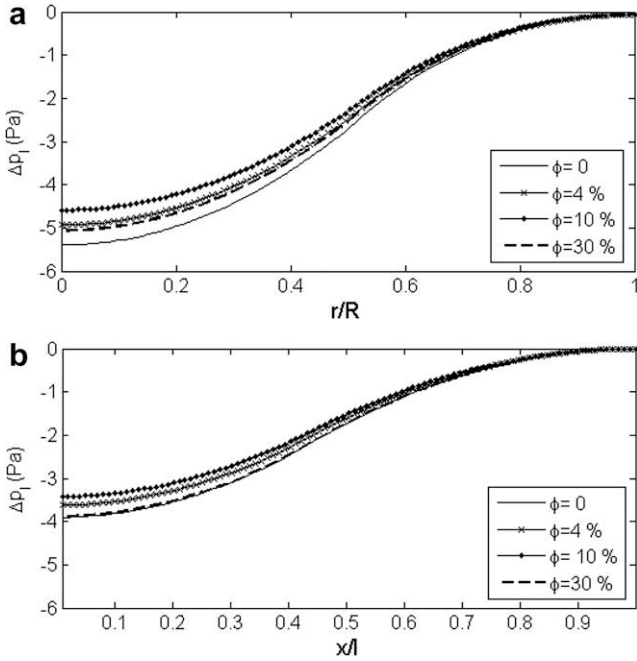
Fig. 2. Liquid pressure distribution for different concentration levels of CuO nanoparticles within the heat pipe; $Q = 9$ kW; (a) disk-shaped heat pipe and (b) rectangular shaped heat pipe.

$$k_{pe} = \frac{[2(1-\alpha) + (1+\beta)^3(1+2\alpha)]\alpha}{-(1-\alpha) + (1+\beta)^3(1+2\alpha)} k_p \quad (15)$$

$$\alpha = \frac{k_{layer}}{k_p}; \quad \beta = \frac{w}{r_p} \quad (16)$$

where k_p and k_{layer} are the thermal conductivities of the nanoparticle and nanolayer, respectively.
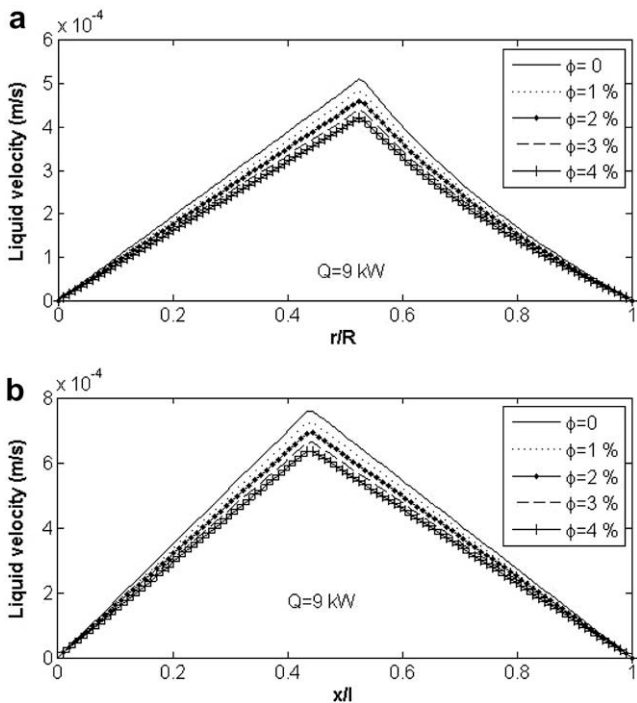
Fig. 3. Liquid velocity profiles for various concentration levels of CuO nanoparticles within the flat heat pipes; (a) disk-shaped heat pipe and (b) rectangular shaped heat pipe, $Q = 9$ kW.
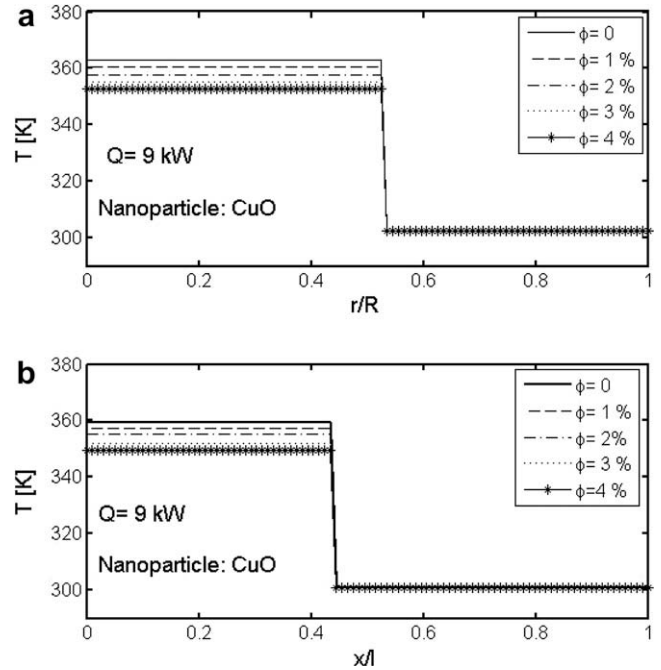
Fig. 4. Heat pipe wall temperature distribution for different nanoparticles concentration levels; $Q = 9$ kW; $d_p = 20$ nm; (a) disk-shaped heat pipe, and (b) rectangular shaped heat pipe.

2.4. Maximum heat transfer capability

For a heat pipe under steady-state operation, capillary pressure of the wick establishes a stable circulation for the working fluid. The maximum heat transport capillary limit of the heat pipe is achieved when the total pressure loss reaches the maximum capillary pressure of the porous wick which can be presented as:
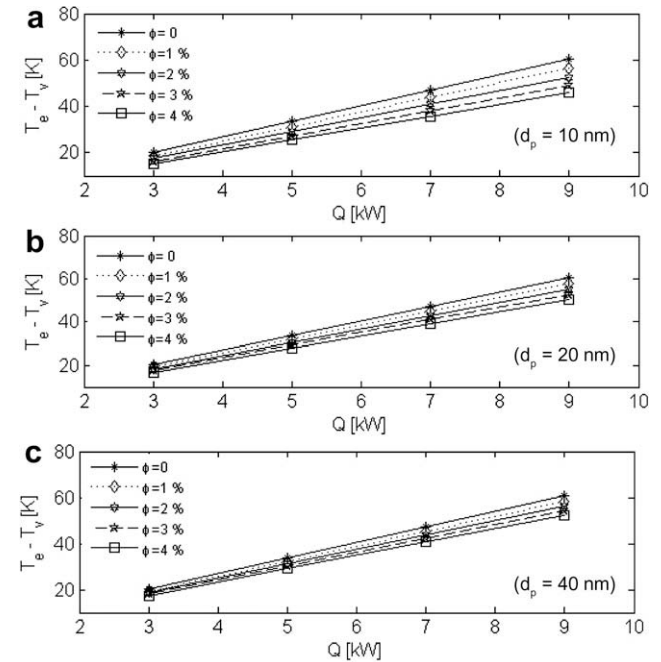
Fig. 5. Temperature difference between evaporator and condenser in disk-shaped heat pipe for different CuO nanoparticle concentration levels, (a) $d_p = 10$ nm, (b) $d_p = 20$ nm and (c) $d_p = 40$ nm.
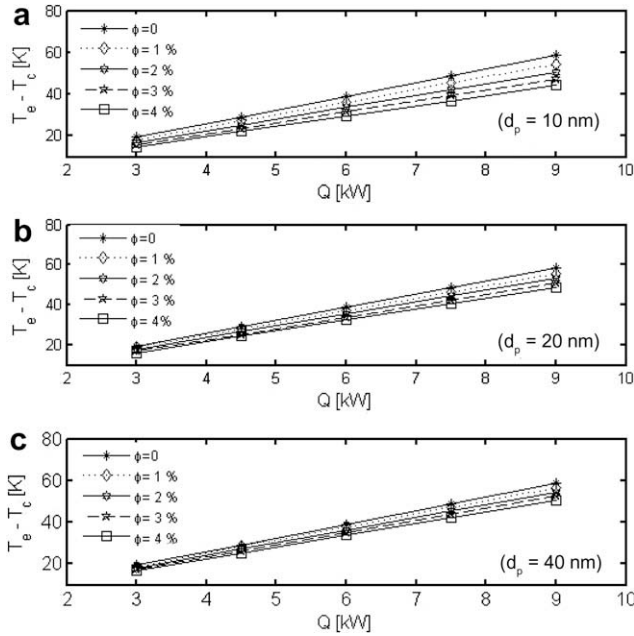
Fig. 6. Temperature difference between evaporator and condenser for the rectangular shaped heat pipe for different CuO concentration levels; (a) d_p = 10 nm, (b) d_p = 20 nm and (c) d_p = 40 nm.

$$\Delta p_{cap} = \Delta p_{v,total} + \Delta p_{l,total} + \Delta p_{g,total} \tag{17}$$

$$(\Delta p_{cap})_{max} = \frac{2\sigma_l}{r_c} \tag{18}$$

where σ_l is the liquid surface tension, and r_c is the effective pore radius of the wick. The total vapor, liquid, and gravitational pressure drops should be less than the maximum capillary pressure head. Neglecting the gravitational head, Eq. (17) can be represented as:

$$(\Delta p_{cap})_{max} \geq \Delta p_{v,total} + \Delta p_{l,total} \tag{19}$$

3. Results and discussion

The analytical models for disk and rectangular shaped heat pipes [2,4] were utilized to study the influence of using a nanofluid on the thermal performance of these heat pipes. Results are obtained for disk and rectangular shaped heat pipes which include nanoparticles within the working fluid. The diameter of the disk-shaped heat pipe is taken equal to the length of the rectangular shaped heat pipe which is 0.46 m for this work. Other nominal dimensions are taken from Vafai and Wang [2] and Vafai et al. [4] works. Three of the most common nanoparticles namely, Al_2O_3, CuO, and TiO_2 with a range of diameters (10, 20 and 40 nm) are utilized to form the nanofluid. The influence of the nanofluid on the liquid pressure, temperature distribution, liquid velocity, temperature gradient, thermal resistance, heat pipe size, and maximum heat removal capability of the flat-shaped heat pipes is investigated.

Fig. 2 displays the liquid pressure distribution for disk and rectangular heat pipes for a range of CuO based nanofluid concentration levels. Initially, the liquid pressure drop decreases by utilizing the nanoparticles within the water due to an increase in density. After reaching a critical concentration level a reversal effect occurs resulting in an increase in the pressure drop as the increase in viscosity of the nanofluid becomes more prominent. The competing effects of the density and viscosity of the nanofluid creates an optimum level of nanoparticle concentration in minimizing the pressure drop for the flat heat pipes.

The influence of nanofluid concentration level on the liquid velocity profile is shown in Fig. 3. An increase in the concentration level decreases the velocity in both disk and rectangular shaped heat pipes. It can be seen through Eqs. (8) and (9) that liquid velocity is inversely proportional to either the density or the viscosity of the liquid.

Fig. 4 displays the wall temperature distribution for flat and disk-shaped heat pipes utilizing the CuO based nanofluid as the working fluid. The input heat and the nanoparticle diameter are 9 kW and 20 nm, respectively. As seen in Fig. 4, the evaporator
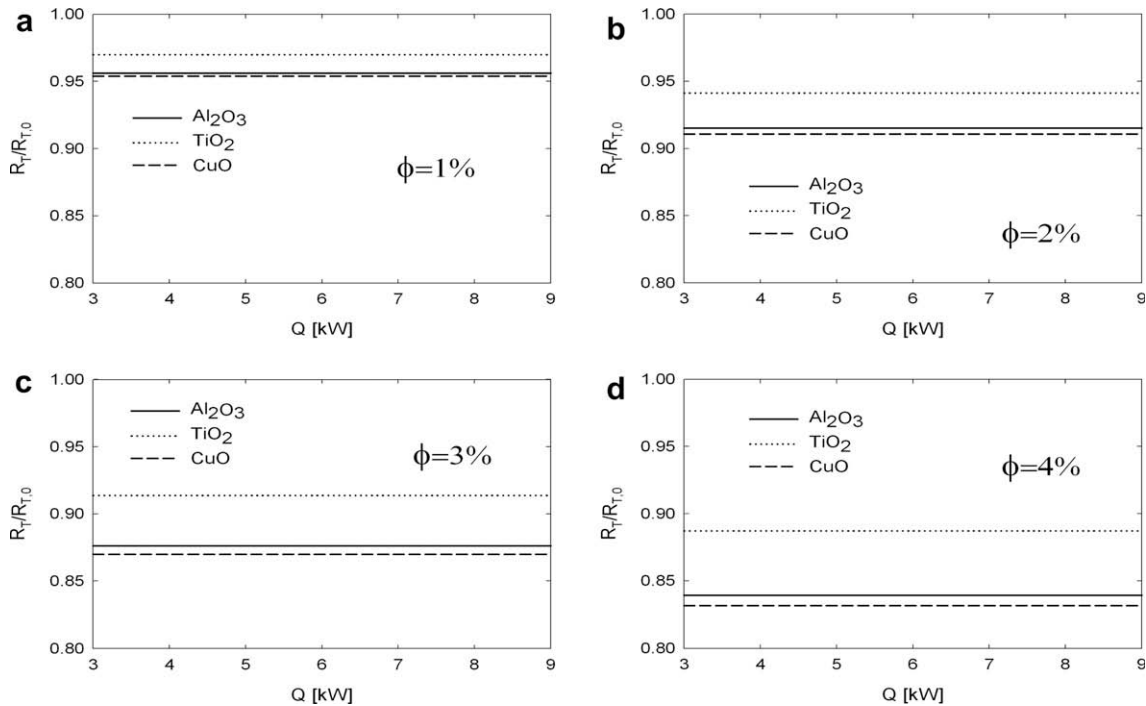
Fig. 7. Effect of nanofluids (d_p = 20 nm) on disk-shaped heat pipe thermal resistance for various heat inputs; (a) ϕ = 1%; (b) ϕ = 2%; (c) ϕ = 3%; (d) ϕ = 4%.
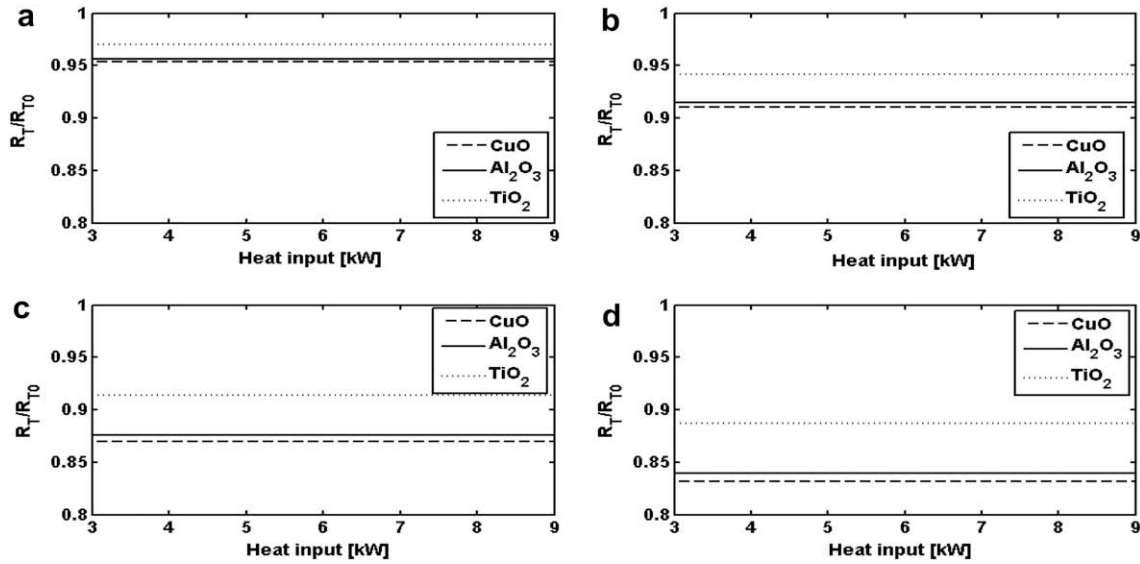
Fig. 8. Effect of nanofluids (d_p = 20 nm) on rectangular shaped heat pipe thermal resistance for various heat inputs; (a) ϕ = 1%; (b) ϕ = 2%; (c) ϕ = 3%; (d) ϕ = 4%.

temperature drops in the presence of nanoparticles. An increase in the concentration level of nanoparticles increases the thermal conductivity of the nanofluid, thus further decreasing the evaporator temperature.

Figs. 5 and 6 show the reduction in the evaporator and condenser temperature difference for different nanoparticle concentration levels for various heat loads. The effect of variations in nanoparticle diameter is also displayed in Figs. 5 and 6. As can be seen the smaller nanoparticle or the larger concentration level the more pronounced the reduction in the temperature difference between the condenser and the evaporator.

Thermal resistance of the flat-shaped heat pipes, defined as $T_e - T_c/Q$, becomes noticeably smaller when a nanofluid is utilized

as seen in Figs. 7 and 8. As seen in these figures, the thermal resistance of a flat-shaped heat pipe can be reduced up to 83% of its initial resistance.

Figs. 9 and 10 demonstrate that using the nanoparticles provides the possibility of a reduction in the size of flat-shaped heat pipe while maintaining the same heat load removal capability. The results are shown for different concentration levels of Al_2O_3, CuO, and TiO_2 with different diameters. For these figures the applied heat input was kept at 9 kW and the evaporator temperature was kept at 90 °C. As can be seen the smallest particle size results in the largest reduction in the size of the heat pipe. For CuO based nanofluid a 30% and 20% reduction in size can be realized for the disk and rectangular shaped heat pipes respectively.
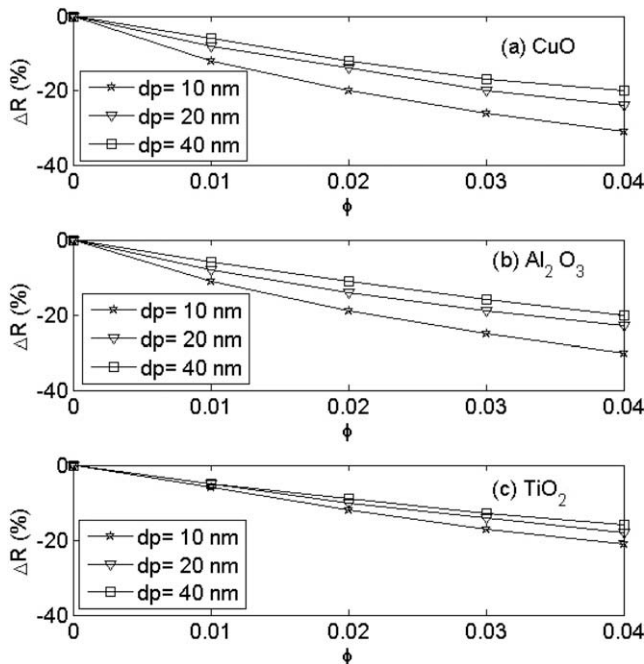
Fig. 9. Percentage reduction level of a disk-shaped heat pipe when using different size nanoparticles and different concentration levels, $T_{evaporator\ wall}$ = 90 °C and Q = 9 kW.
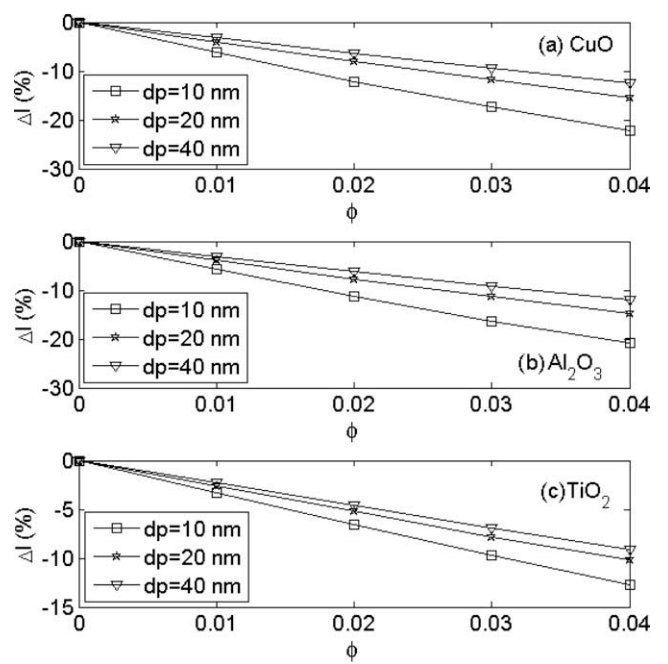
Fig. 10. Percentage reduction level of a rectangular shaped heat pipe when using different size nanoparticles and different concentration levels, $T_{evaporator\ wall}$ = 90 °C and Q = 9 kW.
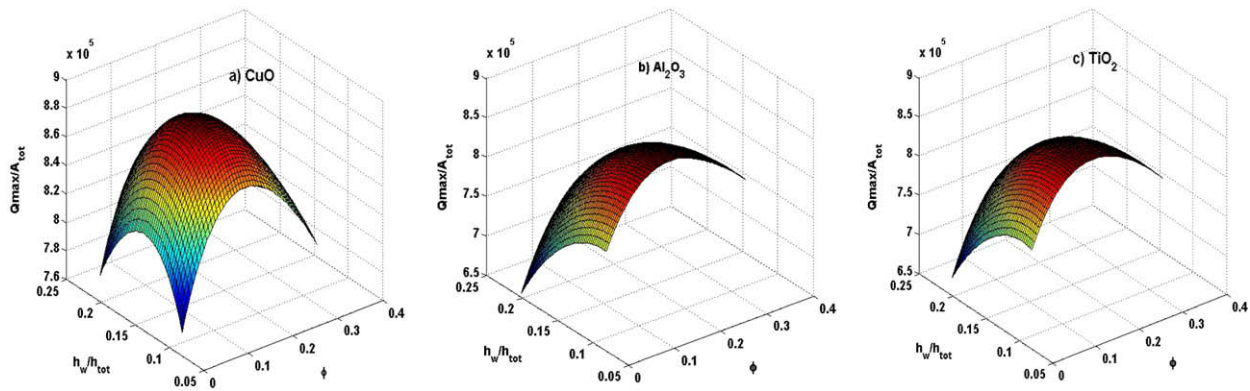
Fig. 11. Three dimensional representation of disk-shaped heat pipe maximum heat removal capability in terms of nanoparticle concentration levels and dimensionless thickness of the wick; (a) CuO, (b) Al_2O_3 and (c) TiO_2.

The effect of changing the wick thickness and nanoparticle concentration level on the maximum heat removal capability of a flat-shaped heat pipe is shown in Fig. 11. The existence of an optimum point for both wick thickness and nanoparticle concentration level can be seen in this figure. The existence of an optimum thickness for the wick was established earlier in the work of Vafai et al. [4]. The appearance of an optimum nanoparticle concentration level based on the competing effects of density and viscosity of the nanofluid level was also established in the work of Shafahi et al. [8] for cylindrical heat pipes.

4. Conclusions

The performance of flat-shaped heat pipes utilizing nanoparticles within the working fluid was investigated in this work. Some of the more widely used nanoparticles, such as Al_2O_3, CuO and TiO_2 with a range of nanoparticle diameters were considered. The flat-shaped heat pipe's liquid pressure, liquid velocity profile, temperature distribution, temperature gradient and maximum heat removal capability were investigated. Furthermore, the possibility of reducing the flat-shaped heat pipe's dimension using a nanofluid, was explored. Results show that the presence of nanoparticles in the working fluid leads to a reduction in the speed of the liquid, smaller temperature difference along the heat pipe and the possibility of reduction in size under the same operational conditions. Using a nanofluid reduces the thermal resistance of the flat-shaped heat pipe similar to what has been observed experimentally. The maximum heat removal capability of the flat-shaped heat pipe was displayed for a range of wick thicknesses and nanoparticles concentration levels. The existence of an optimum nanoparticle concentration level and wick thickness in maximizing the heat removal capability of the flat-shaped heat pipe was established.

References

[1] A. Faghri, Heat pipe Science and Technology, Taylor & Francis, Washington, DC, 1995.
[2] K. Vafai, W. Wang, Analysis of flow and heat transfer characteristics of an asymmetrical flat-plate heat pipe, Int. J. Heat Mass Transfer 35 (1991) 2087–2099.
[3] N. Zhu, K. Vafai, Analytical modeling of the startup characteristics of asymmetrical flat-plate and disk-shaped heat pipes, Int. J. Heat Mass transfer 41 (1998) 2619–2637.
[4] K. Vafai, N. Zhu, W. Wang, Analysis of asymmetric disk-shaped and flat-plate heat pipes, J. Heat Transfer 117 (1995) 209–218.
[5] Y. Wang, K. Vafai, An experimental investigation of the transient characteristics on a flat-plate heat pipe during startup and shutdown operations, ASME J. Heat Transfer 122 (2000) 525–535.
[6] Y. Wang, K. Vafai, An experimental investigation of the thermal performance of an asymmetrical flat plate heat pipe, Int. J. Heat Mass transfer 43 (2000) 2657–2668.
[7] N. Zhu, K. Vafai, Analysis of cylindrical heat pipes incorporating the effects of liquid–vapor coupling and non-Darcian transport – a closed form solution, Int. J. Heat Mass transfer 42 (1999) 3405–3418.
[8] M. Shafahi, V. Bianco, K. Vafai, O. Manca, An investigation of the thermal performance of cylindrical heat pipes using nanofluids, Int. J. Heat Mass Transfer 53 (2010) 376–383.
[9] P. Naphon, D. Thongkum, P. Assadamongkol, Heat pipe efficiency enhancement with refrigerant–nanoparticles mixtures, Energy Convers. Manage. 50 (2009) 772–776.
[10] X.F. Yang, Z.H. Liu, J. Zhao, Heat transfer performance of a horizontal micro-grooved heat pipe using CuO nanofluid, J. Micromechan. Microeng. 18 (2008) 035038.
[11] H.B. Ma, C. Wilson, Q. Yu, K. Park, U.S. Choi, M. Tirumala, An experimental investigation of heat transport capability in a nanofluid oscillating heat pipe, J. Heat Transfer 128 (2006) 1213–1216.
[12] P. Naphon, P. Assadamongkol, T. Borirak, Experimental investigation of titanium nanofluids on the heat pipe thermal efficiency, Int. Commun. Heat Mass Transfer 35 (2008) 1316–1319.
[13] P.D. Shima, J. Philip, B. Raj, Role of microconvection induced by Brownian motion of nanoparticles in the enhanced thermal conductivity of stable nanofluids, Appl. Phys. Lett. 94 (2009) 223101.
[14] Y. Xuan, Y. Huang, L. Qiang, Experimental investigation on thermal conductivity and specific heat capacity of magnetic microencapsulated phase change material suspension, Chem. Phys. Lett. 479 (2009) 264–269.
[15] W. Evans, J. Fish, P. Keblinski, Role of Brownian motion hydrodynamics on nanofluid thermal conductivity, Appl. Phys. Lett. 88 (2006) 093116.
[16] K.B. Anoop, T. Sundararajan, S.K. Das, Effect of particle size on the convective heat transfer in nanofluid in the developing region, Int. J. Heat Mass transfer 52 (2009) 2189–2195.
[17] J. Jung, J.Y. Yoo, Thermal conductivity enhancement of nanofluids in conjunction with electrical double layer (EDL), Int. J. Heat Mass transfer 52 (2009) 525–528.
[18] M. Beck, Y. Yuan, P. Warrier, A.S. Teja, The effect of particle size on the thermal conductivity of alumina nanofluids, J. Nanoparticle Res. 11 (2009) 1129–1136.
[19] K. Fang, C. Weng, S. Ju, An investigation into the structural features and thermal conductivity of silicon nanoparticles using molecular dynamics simulations, Nanotechnology 17 (2006) 3909–3914.
[20] S.W. Kang, W.C. Wei, S.H. Tsai, S.Y. Yang, Experimental investigation of silver nano-fluid on heat pipe thermal performance, Appl. Therm. Eng. 26 (2006) 2377–2382.
[21] S.W. Kang, W.C. Wei, S.H. Tsai, C.C. Huang, Experimental investigation of nanofluids on sintered heat pipe thermal performance, Appl. Therm. Eng. 29 (2009) 973–979.
[22] Y. Chen, W. Wei, S. Kang, C. Yu, Effect of nanofluid on flat heat pipe thermal performance, in: 24th IEEE SEMI-THERM Symposium, 16–19, March 16–20, 2008.
[23] Y. Lin, S. Kang, H. Chen, Effect of silver nano-fluid on pulsating heat pipe thermal performance, Appl. Therm. Eng. 28 (2008) 1312–1317.
[24] Z. Liu, J. Xiong, R. Bao, Boiling heat transfer characteristics of nanofluids in a flat heat pipe evaporator with micro-grooved heating surface, Int. J. Multiphase Flow 33 (2007) 1284–1295.
[25] H.B. Ma, C. Wilson, B. Borgmeyer, K. Park, Q. Yu, S.U.S. Choi, M. Tirumala, Effect of nanofluid on the heat transport capability in an oscillating heat pipe, Appl. Phys. Lett. 88 (2006) 143116.
[26] R. R. Riehl, Analysis of loop heat pipe behavior using nanofluid, in: Heat Powered Cycles International Conference (HPC), New Castle, UK, paper 06102, September 11–14, 2006.
[27] C.Y. Tsaia, H.T. Chiena, P.P. Dingb, B. Chanc, T.Y. Luhd, P.H. Chena, Effect of structural character of gold nanoparticles in nanofluid on heat pipe thermal performance, Mater. Lett. 58 (2004) 1461–1465.

[28] H.C. Brinkman, The viscosity of concentrated suspensions and solution, J. Chem. Phys. 0 (1952) 571–581.

[29] B.C. Pak, Y.I. Cho, Hydrodynamic and heat transfer study of dispersed fluids with submicron metallic oxide particles, Exp. Heat Transfer 11 (1998) 151–170.

[30] S.W. Chi, Heat Pipe Theory and Practice, Hemisphere, Washington, DC, 1976.

[31] W. Yu, S.U.S. Choi, The role of interfacial layers in the enhanced thermal conductivity of nanofluids: a renovated Maxwell model, J. Nanoparticle Res. 5 (2003) 167–171.